Uncertainty Quantification for Basin-Scale Conductive Models

Denise Degen[1], Karen Veroy[2,3], Florian Wellmann[1]

[1]Computational Geoscience and Reservoir Engineering (CGRE), RWTH Aachen University, Wüllnerstraße 2, 52072 Aachen, Germany

[2]Centre for Analysis, Scientific Computing and Applications, Department of Mathematics & Computer Science, Eindhoven University of Technology (TU/e), Groene Loper 5, Eindhoven, The Netherlands

[3]Faculty of Civil Engineering, RWTH Aachen University, Schinkelstraße 2, Aachen, Germany

Key Points:

- We present a novel method to combine geophysical simulations with uncertainty quantification for the entire state.
- By using an physics-based machine learning approach, we preserve the physical laws and maintain prediction capabilities.
- We generate temperature uncertainty maps in a geothermal study, but the methods are equally applicable to other geophysical simulations.

Corresponding author: Denise Degen, `denise.degen@cgre.rwth-aachen.de`

Abstract

Geophysical simulations are commonly used in many scientific studies. Especially in complex simulations, it is still common practice to provide a single deterministic outcome. Often, a probabilistic approach would be preferable, as a way to quantify and communicate uncertainties, but is infeasible due to long simulation times. We present here a method to generate full state predictions based on a reduced basis method that significantly reduces simulation time, thus enabling studies which require a large number of simulations, such as probabilistic simulations and inverse approaches. We implemented this approach in an existing simulation framework and showcase the application in a geothermal study, where we generate 2D and 3D predictive uncertainty maps. These maps allow a detailed model insight, identifying regions with both high temperatures and low uncertainties. Due to the flexible implementation, the methods are transferable to other geophysical simulations, where both the state and the uncertainty are important.

1 Introduction

Geophysical and geoscientific applications have many sources of uncertainties, arising from, for instance, unresolved and unaccounted physical processes, inaccurate geometrical information, and variations in the parameter distributions. Identifying and quantifying these uncertainties is a non-trivial process. Methods that easily require a million forward simulations, as Markov Chain Monte Carlo (MCMC), make this task not only non-trivial but computationally prohibitive for basin-scale geological heat flow models using state-of-the-art finite element solvers.

To address this, the finite element model is replaced by a surrogate model such as Kriging (Miao et al., 2019; Mo et al., 2019), or polynomial chaos expansions (Navarro et al., 2018). The issue with these surrogate models is that they are defined in the observation space only. Values outside this space need to be determined via inter- and extrapolation. For geothermal studies, however, we are interested in the entire temperature distribution at a particular target depth. Therefore, we use a physics-based learning approach, the reduced basis method (RB) (Prud'homme et al., 2002; Veroy et al., 2003; Hesthaven et al., 2016), as the surrogate model. In contrast to other surrogate models, the RB method has the advantage that it retrieves the temperature distribution in the entire model and is not restricted to the observation space.

The utility of model order reduction for Bayesian inversion has been investigated in previous studies (Chen & Schwab, 2015, 2016; Cui et al., 2015; Himpe & Ohlberger, 2015; Galbally et al., 2010; Lieberman et al., 2010; Manzoni et al., 2016). However, these papers focus on the methodology, and the presented case studies do not capture the typical complexity of geothermal basin-scale applications. The work (Elison et al., 2019) investigates the uncertainty of the thermal conductivity via Markov Chain Monte Carlo. The uncertainty for the temperatures are only considered for five realizations and only interpreted on a 2D-Slice. In contrast, we present a global-sensitivity-driven stochastic model calibration for complex basin-scale applications to generate predictive 3D uncertainty maps enhancing the efficiency of geothermal exploration. Furthermore, we consider all realizations obtained by the Markov Chain Monte Carlo analysis for the uncertainty quantification of the temperatures. The workflow is illustrated in Fig. 1. In previous studies, we investigated the construction of surrogate models for a geoscientific context using the RB method (Degen, Veroy, & Wellmann, 2020). Furthermore, we demonstrated in (Degen, Veroy, Freymark, et al., 2020) the benefits of the RB method for basin-scale global sensitivity analysis and deterministic model calibrations.

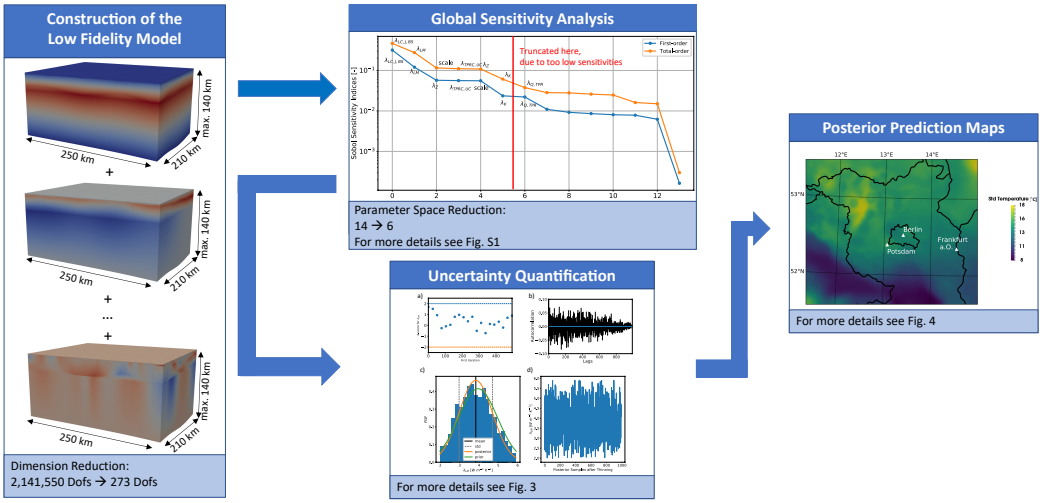

Figure 1. Schematic representation of the workflow.

2 Materials and Methods

In the following section, we briefly introduce the geological model, the governing equations, and the numerical methods used throughout this paper.

2.1 The Brandenburg Model

In this paper, we are using a combination of the Brandenburg models presented in (Noack et al., 2012, 2013). The model (see Fig. 2) has a spatial extent of 250 km in the x-direction, 210 km in the y-direction and extends down to the lithosphere-asthenosphere boundary (LAB). It consists of 17 geological layers and is discretized using tetrahedrons. The upper 11 layers have a horizontal resolution of 0.22 km^2 and a vertical resolution that is interpolated from the z-evaluations of the geological layers. The lower six layers have the same horizontal resolution as the upper 11 layers but the vertical element length corresponds to the layer thickness. This results in a tetrahedron mesh with 2,141,550 degrees of freedom.

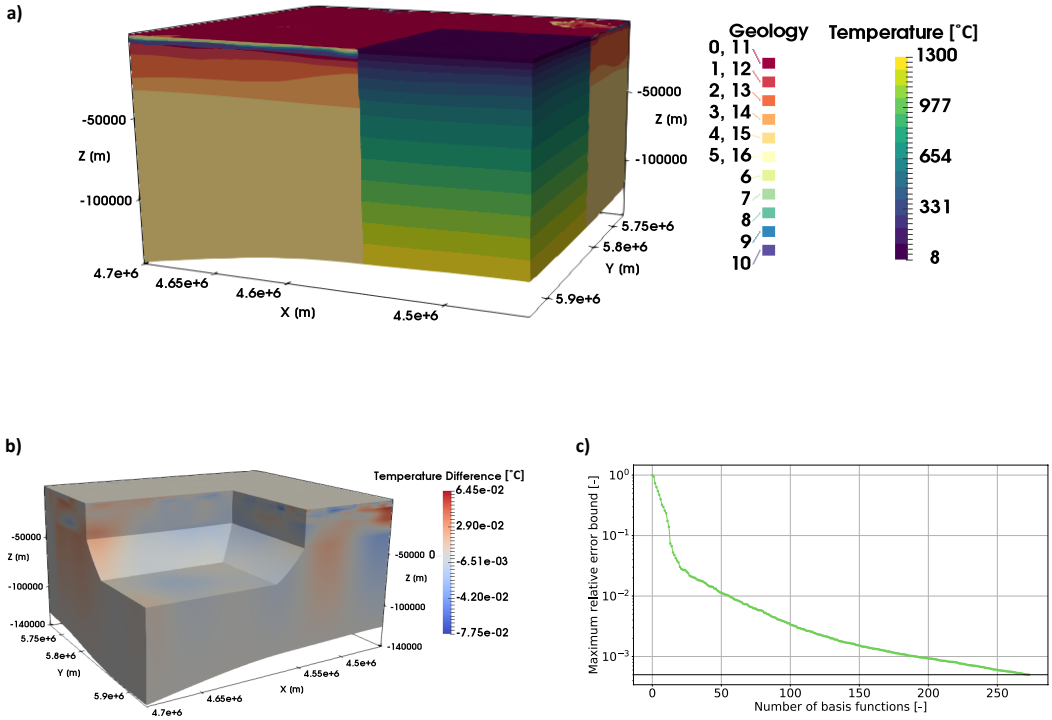

Figure 2. a) Image of the Brandenburg model and the prior temperature distribution. For the layer IDs refer to Table S1. b) The error between the full and reduced model for the prior parameters. c) Convergence of the maximum relative error bound for the entire parameter range.

For the forward simulations, we take a geothermal conduction problem with the radiogenic heat production S as the source term (Bayer et al., 1997):

$$-\lambda \nabla^2 T + S = 0, \tag{1}$$

where λ is the thermal conductivity, and T the temperature. In order to investigate the relative importance of the parameters, and for efficiency reasons, we nondimensionalize the equation, which leads to Eq. 2:

$$-\frac{\lambda}{\lambda_{\mathrm{ref}}\, S_{\mathrm{ref}}}\,\frac{\nabla^2}{l_{\mathrm{ref}}^2}\left(\frac{T-T_{\mathrm{ref}}}{T_{\mathrm{ref}}}\right) + \frac{S\, l_{\mathrm{ref}}^2}{S_{\mathrm{ref}}\, T_{\mathrm{ref}}\, \lambda_{\mathrm{ref}}} = 0 \tag{2}$$

Here, we chose the maximum thermal conductivity of the Brandenburg model of 3.95 W m^{-1} K^{-1} as reference thermal conductivity λ_{ref}. The maximum temperature of 1300 °C is the reference temperature T_{ref}, the maximum radiogenic heat production (2.5 μW m^3) is the reference radiogenic heat production S_{ref}. The reference length l_{ref} corresponds to the maximum x-extent of all models (250,000 m). At the top of the model, we apply a Dirichlet boundary condition of 8 °C, corresponding to the average annual temperature, and at the base of the LAB a Dirichlet boundary condition of 1300 °C (Turcotte & Schubert, 2002). Additionally, we allow a scaling of the lower boundary condition of ± 10 % to account for errors in the geometric description of the LAB. All thermal properties are summarized in Table S1 and the weak form of Eq. 2 is presented in Text S2.

For the validation of the models, we are using the bottom-hole temperature measurements presented in (Noack et al., 2012, 2013) and corrected after (Förster, 2001). The values for the thermal conductivity and the radiogenic heat production are taken from (Noack et al., 2012, 2013) and are originating from previous model studies after (Bayer et al., 1997). Throughout this paper, we vary only the thermal conductivities, whereas the radiogenic heat production values are kept constant since the radiogenic heat productions have a minor effect on the temperature distribution at the target depth in comparison to the thermal conductivities. We further reduce the number of involved parameters in the reduction and inverse processes by combining layers with equal thermal conductivities into one, as presented in Table S1.

2.2 Brandenburg – Reduced Model

We construct a surrogate model using the RB method based on the full FE model. The RB method is a model order reduction technique that aims at significantly reducing the spatial and temporal degrees of freedom of, for instance, finite element problems. For further information regarding the method please refer to (Prud'homme et al., 2002; Veroy et al., 2003; Quarteroni et al., 2015; Hesthaven et al., 2016), and for more infor-

mation on the RB method in the context of Geosciences refer to (Degen, Veroy, & Wellmann, 2020). The geothermal problem, described in Eq. 1, is affine decomposable, meaning separable into a parameter-independent and -dependent part.

The RB method takes advantage of this affine decomposition in an offline-online procedure. During the offline stage, performed only once, all expensive pre-computations for the basis construction are performed. The construction of the basis is achieved via a greedy algorithm (Veroy et al., 2003), which involves training or "learning" of the low-dimensional model. In contrast to machine learning approaches, we are not training based only on data but instead on the physical model.

On the other hand, the online stage uses only the reduced model. Hence, it for the given example several orders of magnitude faster than the original FE model making it advantageous for "outer loop" processes, such as calibrations and uncertainty quantification.

3 Results

For the uncertainty quantification of the Brandenburg model, we perform a Markov Chain Monte Carlo analysis (Iglesias & Stuart, 2014) with a Metropolis sampling using the Python library PyMC (Patil et al., 2010). A previously performed Sobol sensitivity analysis with the Saltelli sampler and 300,000 forward solves showed that the model is insensitive to eight of the 14 parameters (Fig. S1). We thus reduce the parameter dimension from 14 parameters to six. For more information regarding global sensitivity analyses, refer to (Sobol, 2001; Degen, Veroy, Freymark, et al., 2020).

For all thermal conductivities in the sensitivity analysis and the MCMC algorithm, we allow a variation of $\pm$ 50 %. The number of function evaluations for the MCMC run is set to 1,000,000 with a thinning of 1,000 and 10,000 burn-in-simulations. For the priors, we use normally distributed parameters. The mean of each parameter corresponds to the fitted thermal conductivity values of (Noack et al., 2012, 2013). Both the standard deviation and proposal standard deviation are set to:

- one for the Tertiary-pre-Rupelian-clay/Upper Cretaceous and Lower Cretaceous/Jurassic layer
- two for the Keuper layer

- four for the Zechstein layer and the Lithospheric Mantle
- 0.002 for the scaling parameter of the lower boundary condition

and are afterwards divided by their respective mean values. The standard deviations have been determined such that the values do not exceed a range of ± 50 % of their mean values to ensure physical plausibility. Analog to the deterministic model calibration, we use the temperature data presented in (Noack et al., 2012, 2013). The bottom-hole temperatures of this database have been measured during the drilling process and were later on corrected after (Förster, 2001). This correction might not fully capture the perturbation of the temperature field. Therefore, we apply a standard deviation of 2 % for the observation data.

3.1 Thermal Conductivities

Now, we discuss the posterior distribution of the thermal conductivities obtained by the MCMC analysis (Tab. S1). Through a Quantile-Quantile analysis (Fig. S2), we determined that the normal distributions describe our parameter quite well. Hence, we discuss in the following only the posterior mean and standard deviations of the thermal conductivities.

We obtain for the Tertiary Rupelian-clay/Upper Cretaceous layer (Fig. S4), a slight increase in the posterior mean thermal conductivity of 0.05 W m^{-1} K^{-1} in contrast to the prior thermal conductivity. The parameter follows a normal distribution with a standard deviation of 0.47 W m^{-1} K^{-1}. We observe a posterior thermal conductivity of:

- 2.11 W m^{-1} K^{-1} ± 0.45 W m^{-1} K^{-1} for the Lower Cretaceous/Jurassic/Buntsandstein layer (Fig. S5),
- 2.35 W m^{-1} K^{-1} ± 0.58 W m^{-1} K^{-1} for the Keuper layer (Fig. S6),
- and 3.56 W m^{-1} K^{-1} ± 0.81 W m^{-1} K^{-1} for the Zechstein layer (Fig. S7).

Hence, all three cases show an increase in the posterior thermal conductivity in comparison to the prior thermal conductivity, and they are also normally distributed. The Lithospheric Mantle shows a decrease in the posterior mean thermal conductivity of 0.11 W m^{-1} K^{-1} in comparison to the prior thermal conductivity and has a posterior standard deviation of 0.86 W m^{-1} K^{-1} (Fig. 3). The scaling parameter (Fig. S8) has a posterior mean value of 1.00, which is identical to the prior value, and a posterior standard deviation of 0.04.

All parameters follow a normal distribution and a autocorrelation around zero. The z-scores (Figure 3a, S4a - S8a) indicated converges for all chains. The z-scores measure the mean and the variance of the entire chain. The execution of the MCMC algorithm took in total about 4.5 hours, for the one Million forward solves.

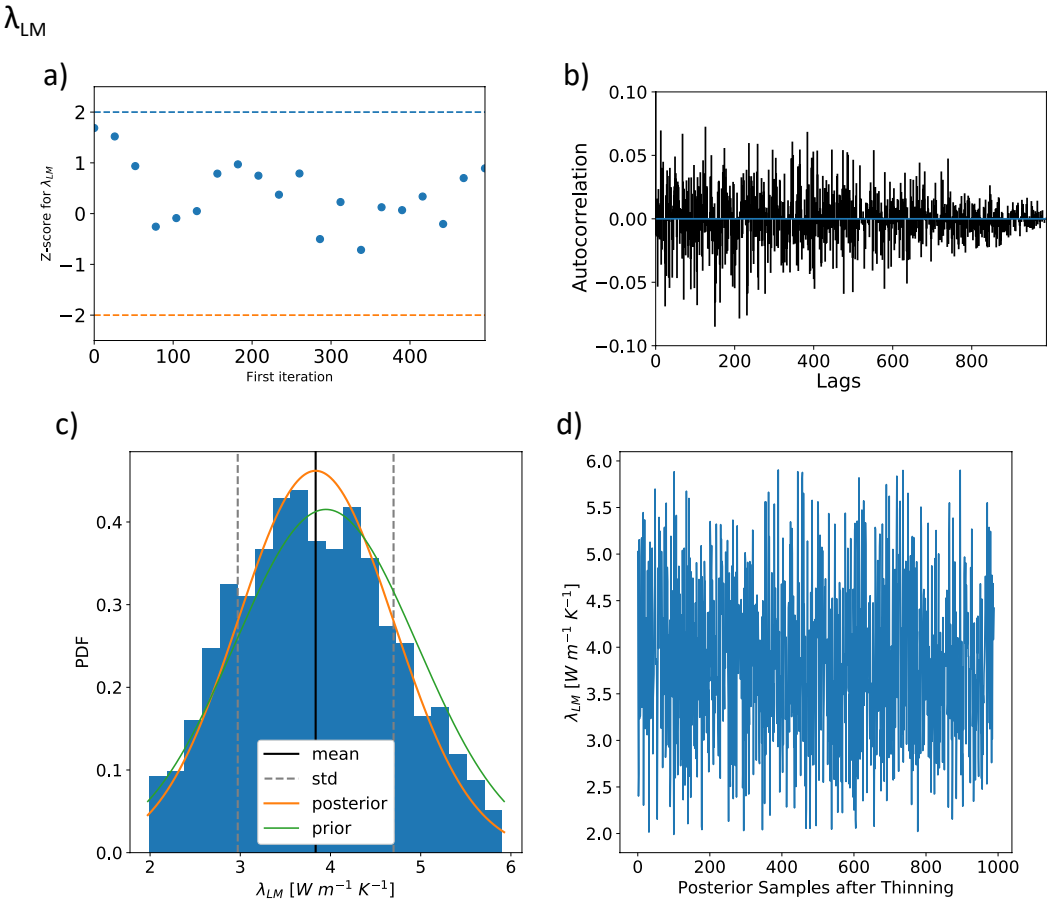

Figure 3. Posterior Analysis of the Lithospheric Mantle (LM). Shown are the a) Geweke Plot b) autocorrelation, c) posterior parameter distributions, and d) the trace.

3.2 Uncertainty Quantification Maps

First, we use the parameter distributions of the MCMC analysis to generate 2D and 3D uncertainty quantification maps. We make here also use of the RB method, which allows us to compute model realizations for samples from the posterior distribution to obtain temperature state values everywhere in space.

For the generation of uncertainty quantification maps, we first have to choose a suitable representation. A Quantile-Quantile analysis (Fig. S3) for nine points at a depth of 5 km shows that the temperature is normally distributed. Hence, we plot in the following the posterior mean temperatures and their standard deviations to achieve a suitable representation of the temperature uncertainties.

First, we present the posterior distributions in the entire Brandenburg model. The posterior standard deviations have their highest value within the sedimentary basin at a depth of about 30 to 35 km (see Fig. 4a). Consequently, the highest uncertainties also occur there. Overall, we observe uncertainties ranging from 0 °C to 53 °C. We observe that the uncertainty decreases towards the boundaries and increases towards the center part of the model. The gradient of the posterior mean temperature distribution is steep in the upper part of the model and a significantly less steep gradient in the lower part of the model. The temperatures range from 8 °C to 1300 °C (see Fig. 2).

Now, we focus on the posterior distributions at a typical target depth for geothermal systems of 5 km. The posterior mean temperature ranges from 141 °C to 197 °C, and the posterior standard deviation from 8 °C to 18 °C. The highest uncertainty, in a depth of 5 km, is north of the interface of the Tertiary-post-Rupelian and the Rupelian clay and south to the Zechstein - Sedimentary Rotliegend interface. The area is marked with an A in Fig. 4c. It has its highest peak southeast to the region, where salt structures majorly influence the posterior mean temperatures. Generally, from the interface (marked with a B), the uncertainties increase towards the north and decrease towards the south of the model.

The highest posterior mean temperatures of over 190 °C are north of the interface of the Tertiary-post-Rupelian and the Rupelian clay (marked with a C). In contrast, the lowest posterior mean temperature values around 140 °C are south of this interface (see B in Fig. 4b). In general, the posterior mean temperature north of the interface decrease to the northern border of the model. Furthermore, in the north-west part of Brandenburg, a region of lower posterior mean temperatures is located (area A in Fig. 4b). The reasons for this decreased posterior mean temperature will be discussed in Section 4.2.

3.3 Computational Cost

The reduction requires 273 basis functions for reaching the pre-defined relative error tolerance of $5 \cdot 10^{-4}$ for the nondimensional model (see Fig. 2c). Note that the most accurate measurements have an accuracy of 10^{-1}. Consequently, the chosen error tolerance ensures that we do not introduce approximation errors above the measurement error. The reduced basis method leads to a speed-up of $1.0 \cdot 10^{5}$.

4 Discussion

A benefit of the methodology presented here is the generation of predictive uncertainty quantification maps, enabled by using the RB method as a surrogate model. Therefore, we are able to reveal important insights into the spatial distribution of the uncertainties. Other surrogate models would not allow the generation of predictive uncertainty maps since they are limited to the observation space.

4.1 Thermal Conductivities

To discuss the uncertainties related to the thermal conductivities, we first focus on the posterior mean thermal conductivities. The posterior mean thermal conductivities of all layers show only a slight deviation from the prior thermal conductivities. This is not surprising since they are coming from previous model studies and are therefore already quite well adapted to the model. If we compare them to the measured thermal conductivities presented in (Noack et al., 2012), we observe an apparent deviation.

Even though the posterior mean thermal conductivities are in a good agreement with the prior thermal conductivities, the need for uncertainty quantification becomes apparent through the posterior standard deviation. For all layers, we observe large posterior standard deviations for the thermal conductivity, meaning that we have high uncertainties for all layers. The uncertainty in the parameters is mainly influenced by the uncertainty of the observation data and by the upper boundary condition. In our study, we place a lot of trust in the data. Still, we allow variations from that data set since we are operating with partially corrected bottom-hole temperatures. We assume that the correction factor is not able to fully compensate for the perturbation of the temperature field during the drilling process, resulting in slightly uncertain observation data. The posterior standard deviation decreases by putting more trust in the observation data. There-

fore, temperature observations that are performed when the temperature field is in equilibrium would significantly improve the certainty of the different thermal conductivities.

Except for the Lithospheric Mantle, all posterior mean thermal conductivities show an increase in comparison to the prior thermal conductivity. Since the layers above the salt show an increase in the posterior thermal conductivity and the layer below shows a decrease, that might be an indication that some salt structures were not resolved. The stochastic calibration demonstrates that a geothermal conduction problem adequately describes the sedimentary basin of Brandenburg. Furthermore, the small posterior standard deviation of the scaling parameter for the lower boundary condition shows that the boundary is placed far enough from the area of interest to avoid any interference.

4.2 Uncertainty Quantification Maps

We first focus on the uncertainties associated with the temperatures in the entire Brandenburg model. The distribution of these uncertainties seems to be contradictory to our expectations. Usually, one expects an increasing uncertainty with depth. We observe a decreasing uncertainty towards the boundaries and an increasing uncertainty towards the center part of the model instead. Both for the top and the bottom boundary condition, we apply Dirichlet boundary conditions, where the upper boundary condition has a value of 8 °C throughout all simulations. The lower boundary condition varies by a factor of $\pm$ 10 %. We allow this variation to account for geometrical parameterization errors of the LAB. This is the reason why we observe decreasing uncertainties towards these boundary conditions because the values of the boundaries are relatively fixed within all simulations. The highest uncertainties are between 30 km and 35 km depth, where no interactions of the boundary conditions are observable.

We can also use the distribution of the uncertainties to investigate the influence of the respective boundary conditions. Although the LAB is at a depth varying from approximately 100 km to 140 km, the boundary significantly influences the model up to a depth of 80 km to 100 km. For our investigations, this is uncritical since our target depth is at 5 km depth. Nonetheless, this demonstrates that it is essential to have a vertical extent that is significantly larger than the target depth. The upper boundary condition is influencing the model to a depth of 10 km, meaning that the upper boundary condition significantly affects our target depth.

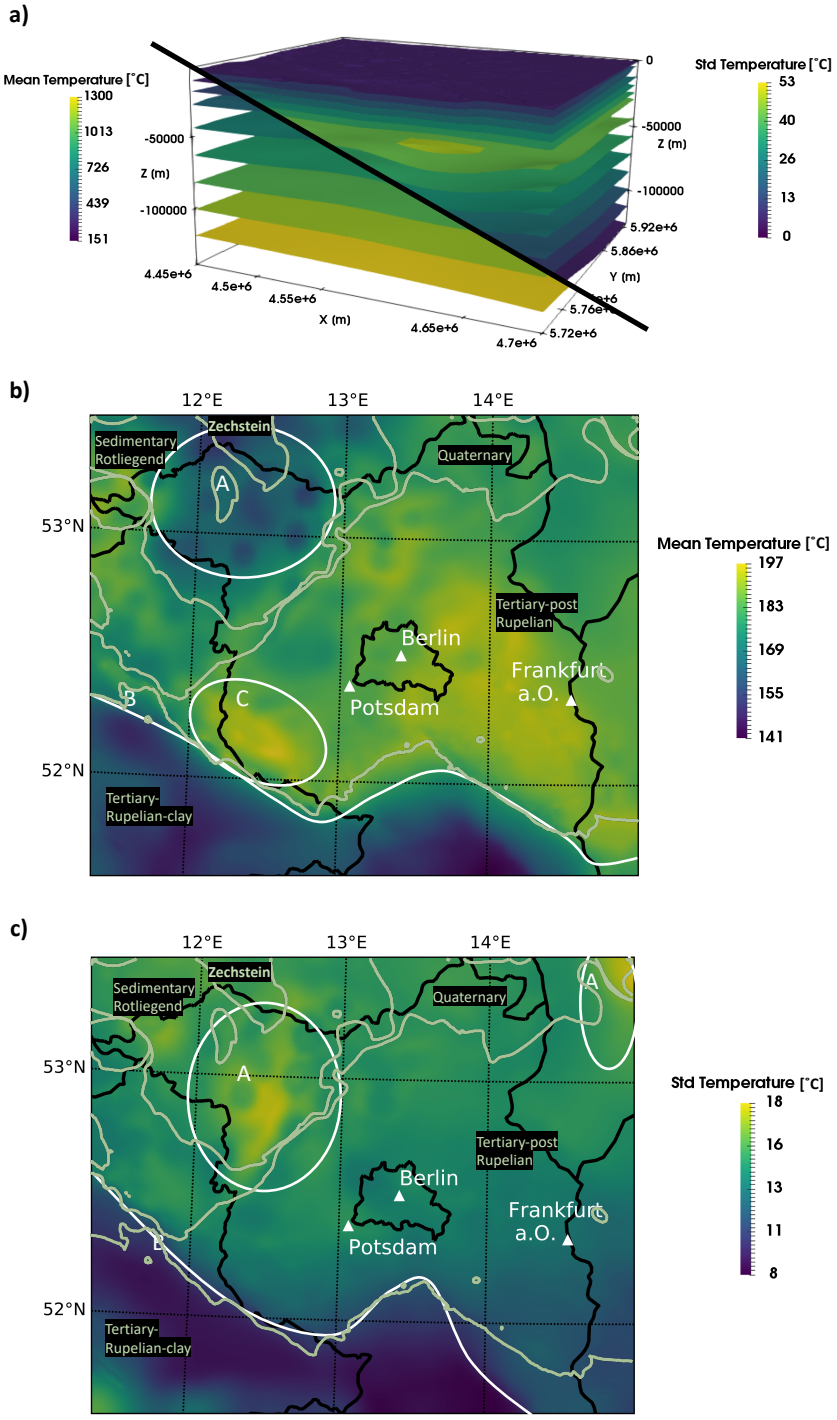

Figure 4. a) Distribution of the posterior mean temperature and the posterior standard deviation of the entire Brandenburg model. b) Map of the posterior mean temperature and c) posterior standard deviation at the target depth of 5 km. The light green lines in b) and c) indicate the boundaries of the geological layers

This is not avoidable since the surface naturally defines the upper boundary. However, this is less critical than the influence of the lower boundary condition because we can determine the upper boundary with a much higher certainty than the lower. Nonetheless, it shows that it is crucial to characterize the upper boundary condition with great detail.

At the target depth, the highest uncertainties are in area A. Hence, they are north of the Tertiary-post-Rupelian and the Rupelian clay (interface B), and south of the Sedimentary Rotliegend and Zechstein interface. The reason is that the variations of the contrast in thermal conductivity are high at these interfaces. Note that the Rupelian clay has a posterior mean thermal conductivity of 1.93 W m^{-1} K^{-1} with a posterior standard deviation of 0.53 W m^{-1} K^{-1} and the Zechstein layer a posterior thermal conductivity of 3.60 ± 0.96 W m^{-1} K^{-1}. Furthermore, the highest uncertainties are adjacent to the region of the salt structures, further emphasizing the influence of the Zechstein layer on the uncertainties. At the target depth, we consider only the Rupelian clay and the Zechstein layer as uncertain and do not include other layers in the uncertainty quantification. The sensitivity analysis shows that the model is insensitive to these parameters. Consequently, the observed uncertainty is arising from the contrast in thermal conductivity between the Rupelian clay- Zechstein layer and the remaining layers.

The posterior mean temperatures at a depth of 5 km are higher north from the Tertiary-post-Rupelian and the Rupelian clay interface (marked with the letter B in Fig. 3b) because the Tertiary-post-Rupelian has a lower thermal conductivity than the Rupelian clay. The colder posterior mean temperature values in the north-western part of the model (area A in Fig. 3b) are coming from the high thermal conductivity of the Zechstein layer. It is further emphasized by the round dome structures in the temperature distribution that are typical for salt. The posterior mean temperature after the stochastic model calibration only slightly deviates from the prior temperature distribution since the changes in the posterior mean thermal conductivity are also minor.

4.3 Reduced Order Model

Note that the usage of a physics-based learning approach has considerable advantages for geothermal and many other geophysical applications. This is caused by the sparsity of the observation data. The data sparsity makes data-driven approaches in many

geophysical applications prohibitive. Instead of training using data, we use the physical model and are therefore able to overcome the problem with the data sparsity.

The RB method requires 5.4 h for the offline stage, using two Intel Xeon Platinum 8160 CPUs (24 cores, 2.1 GHz, 192 GB of RAM) and 4.5 h for the MCMC method. Note that with the finite element method, we would need over 16 core-a.

5 Conclusion and Outlook

We presented an uncertainty quantification at the basin-scale with the generation of uncertainty quantification maps. This is computationally possible since we replace the finite element forward simulation by the reduced basis forward simulation. This results in a reduction of computation time from a couple of hundred seconds to a few milliseconds, and hence in a speed-up of five orders of magnitude. Therefore, we are able to efficiently perform both global sensitivity and MCMC analyses. Because we consider not only the deterministic but the stochastic temperature distribution, we are able to predict the temperatures more reliably. For future work, it would be interesting to incorporate these temperature uncertainties into the economic evaluation of potential geothermal wells. It would be also interesting to investigate the effects of different observation data qualities on the uncertainty of the model temperature distributions.

Acknowledgments

We like to acknowledge Prof. Dr. Magdalena Scheck-Wenderoth and Dr. Vera Noack for providing and generating the Brandenburg model. Furthermore, we would like to acknowledge the funding provided by the DFG through DFG Project GSC111.

The temperature data used throughout this paper is available in (Noack et al., 2012, 2013). For the construction of the reduced models, we used the software package DwarfElephant (Degen, Veroy, & Wellmann, 2020). The software, which is based on the finite element solver MOOSE (Alger et al., 2019), is freely available on GitHub (`https://github.com/cgre-aachen/DwarfElephant`). The sensitivity analyses are performed with the Python library SALib (Herman & Usher, 2017) and the uncertainty quantification with the PyMC library (Patil et al., 2010).

References

Alger, B., Andrš, D., Carlsen, R. W., Gaston, D. R., Kong, F., Lindsay, A. D., ... Stogner, R. (2019). *MOOSE Web page.* `https://mooseframework.org`. Retrieved from `https://mooseframework.org`

Bayer, U., Scheck, M., & Koehler, M. (1997). Modeling of the 3D thermal field in the northeast German basin. *Geologische Rundschau*, *86*(2), 241–251.

Chen, P., & Schwab, C. (2015). Sparse-grid, reduced-basis Bayesian inversion. *Computer Methods in Applied Mechanics and Engineering*, *297*, 84–115.

Chen, P., & Schwab, C. (2016). Sparse-grid, reduced-basis Bayesian inversion: Nonaffine-parametric nonlinear equations. *Journal of Computational Physics*, *316*, 470–503.

Cui, T., Marzouk, Y. M., & Willcox, K. E. (2015). Data-driven model reduction for the Bayesian solution of inverse problems. *International Journal for Numerical Methods in Engineering*, *102*(5), 966–990.

Degen, D., Veroy, K., Freymark, J., Scheck-Wenderoth, M., & Wellmann, F. (2020, Apr). *Global Sensitivity Analysis to Optimize Basin-Scale Conductive Model Calibration - Insights on the Upper Rhine Graben.* EarthArXiv. Retrieved from `eartharxiv.org/b7pgs` doi: 10.31223/osf.io/b7pgs

Degen, D., Veroy, K., & Wellmann, F. (2020). Certified reduced basis method in geosciences. *Computational Geosciences*, *24*(1), 241–259.

Elison, P., Niederau, J., Vogt, C., & Clauser, C. (2019). Quantification of thermal conductivity uncertainty for basin modeling. *AAPG Bulletin*, *103*(8), 1787–1809.

Förster, A. (2001). Analysis of borehole temperature data in the Northeast German Basin: continuous logs versus bottom-hole temperatures. *Petroleum Geoscience*, *7*(3), 241–254.

Galbally, D., Fidkowski, K., Willcox, K., & Ghattas, O. (2010). Non-linear model reduction for uncertainty quantification in large-scale inverse problems. *International journal for numerical methods in engineering*, *81*(12), 1581–1608.

Herman, J., & Usher, W. (2017). Salib: an open-source python library for sensitivity analysis. *J. Open Source Softw*, *2*(9), 97.

Hesthaven, J. S., Rozza, G., Stamm, B., et al. (2016). *Certified reduced basis methods for parametrized partial differential equations.* SpringerBriefs in Mathemat-

ics, Springer.

Himpe, C., & Ohlberger, M. (2015). Data-driven combined state and parameter reduction for inverse problems. *Advances in Computational Mathematics*, *41*(5), 1343–1364.

Iglesias, M., & Stuart, A. M. (2014). Inverse Problems and Uncertainty Quantification. *SIAM News*, 2–3.

Lieberman, C., Willcox, K., & Ghattas, O. (2010). Parameter and State Model Reduction for Large-Scale Statistical Inverse Problems. *SIAM Journal on Scientific Computing*, *32*(5), 2523–2542.

Manzoni, A., Pagani, S., & Lassila, T. (2016). Accurate Solution of Bayesian Inverse Uncertainty Quantification Problems Combining Reduced Basis Methods and Reduction Error Models. *SIAM/ASA Journal on Uncertainty Quantification*, *4*(1), 380–412.

Miao, T., Lu, W., Lin, J., Guo, J., & Liu, T. (2019). Modeling and uncertainty analysis of seawater intrusion in coastal aquifers using a surrogate model: a case study in Longkou, China. *Arabian Journal of Geosciences*, *12*(1), 1.

Mo, S., Shi, X., Lu, D., Ye, M., & Wu, J. (2019). An adaptive Kriging surrogate method for efficient uncertainty quantification with an application to geological carbon sequestration modeling. *Computers & Geosciences*.

Navarro, M., Le Maître, O. P., Hoteit, I., George, D. L., Mandli, K. T., & Knio, O. M. (2018). Surrogate-based parameter inference in debris flow model. *Computational Geosciences*, *22*(6), 1447–1463.

Noack, V., Scheck-Wenderoth, M., & Cacace, M. (2012). Sensitivity of 3D thermal models to the choice of boundary conditions and thermal properties: a case study for the area of Brandenburg (NE German Basin). *Environmental Earth Sciences*, *67*(6), 1695–1711.

Noack, V., Scheck-Wenderoth, M., Cacace, M., & Schneider, M. (2013). Influence of fluid flow on the regional thermal field: results from 3D numerical modelling for the area of Brandenburg (North German Basin). *Environmental earth sciences*, *70*(8), 3523–3544.

Patil, A., Huard, D., & Fonnesbeck, C. J. (2010). PyMC: Bayesian stochastic modelling in Python. *Journal of statistical software*, *35*(4), 1.

Prud'homme, C., Rovas, D. V., Veroy, K., Machiels, L., Maday, Y., Patera, A. T.,

& Turinici, G. (2002). Reliable real-time solution of parametrized partial differential equations: Reduced-basis output bound methods. *Journal of Fluids Engineering*, *124*(1), 70–80.

Quarteroni, A., Manzoni, A., & Negri, F. (2015). *Reduced Basis Methods for Partial Differential Equations: An Introduction*. Springer International Publishing.

Sobol, I. M. (2001). Global sensitivity indices for nonlinear mathematical models and their Monte Carlo estimates. *Mathematics and computers in simulation*, *55*(1-3), 271–280.

Turcotte, D. L., & Schubert, G. (2002). *Geodynamics*. Cambridge university press.

Veroy, K., Prud'homme, C., Rovas, D. V., & Patera, A. T. (2003). A posteriori error bounds for reduced-basis approximation of parametrized noncoercive and nonlinear elliptic partial differential equations. In *Proceedings of the 16th aiaa computational fluid dynamics conference* (Vol. 3847, pp. 23–26).